of Maxwell (*18*) and Feynman (*19*), devices with nanoscale dimensions may actually approach the limit of the second law of thermodynamics, be they mechanically (*20*) or electrically (*21*) driven. Our results point the way for the creation of such a mechanical "ratchet and pawl" device, although the asymmetric periodic profile in our experiment here may not be sufficiently strong at room temperature to ensure the necessary conditions for a completely unidirectional rotation of the molecular rotor (*17*). The rotor (or the cavity) has to be reengineered to optimize the supramolecular ratchet-bushing interaction. In this case, to drive the rotor unidirectionally by thermal means, an additional input is required to increase the rotor potential energy over the ratchet potential barrier at pseudorandom time intervals (*14, 17*). For example, a tunnel current input on the bearing will inelastically heat the rotor (*22*), thus providing a method to rectify thermal noise.

Our results open the way to fabricate, spatially define, and test recent proposals involving mechanical devices fabricated in molecular structures. They raise interesting questions concerning the fundamentals of mechanics in molecular and supramolecular systems, including the role of thermal noise and the design of molecular devices.

References and Notes
1. R. T. Howe, R. S. Muller, K. J. Gabriel, W. S. N. Trimmer, *IEEE Spectrum* **27**, 29 (1990).
2. H. Noji, R. Yasuda, M. Yoshida, K. Kinosita, *Nature* **386**, 299 (1997); H. Miyata *et al.*, *Biophys. J.* **68**, 286S (1995).
3. A. Ishijima *et al.*, *Biochem. Biophys. Res. Commun.* **199**, 1057 (1995); S. M. Block, *Nature* **386**, 217 (1997).
4. K. E. Drexler, *Nanosystems: Molecular Machinery, Manufacturing, and Computation* (Wiley, New York, 1995); D. H. Robertson, B. I. Dunlap, D. W. Brenner, J. W. Mintmire, C. T. White, *Mater. Res. Soc. Symp. Proc.* **349**, 283 (1994); K. Sohlberg, R. E. Tuzun, B. G. Sumpter, D. W. Nold, *Nanotechnology* **8**, 103 (1997).
5. D. M. Ho and R. A. Pascal Jr., *Chem. Mater.* **5**, 1358 (1993).
6. C. Chavy, C. Joachim, A. Altibelli, *Chem. Phys. Lett.* **214**, 569 (1993).
7. T. A. Jung, R. R. Schlittler, J. K. Gimzewski, *Nature* **386**, 696 (1997).
8. J. K. Gimzewski, T. A. Jung, M. T. Cuberes, R. R. Schlittler, *Surf. Sci.* **386**, 101 (1997).
9. M. T. Cuberes, R. R. Schlitter, T. A. Jung, K. Schaumburg, J. K. Gimzewski, *ibid.* **383**, 37 (1997).
10. S. J. Stanick, M. M. Kamna, P. S. Weiss, *Science* **266**, 99 (1994).
11. P. L. Anelli, N. Spencer, J. F. Stoddart, *J. Am. Chem. Soc.* **113**, 5131 (1991).
12. R. Ballardini *et al.*, *Angew. Chem. Int. Ed. Engl.* **32**, 1301 (1993).
13. A. Livoreil, C. O. Dietrich-Buchecker, J. P. Sauvage, *J. Am. Chem. Soc.* **116**, 9399 (1994).
14. M. O. Magnasco, *Phys. Rev. Lett.* **71**, 1477 (1993).
15. R. D. Astumian and M. Bier, *ibid.* **72**, 1766 (1994).
16. T. R. Kelly, I. Tellitu, J. P. Sestelo, *Angew. Chem. Int. Ed. Engl.* **36**, 1866 (1997).
17. R. D. Astumian, *Science* **276**, 917 (1997).
18. H. S. Leff and A. F. Rex, Eds., *Maxwell's Demon: Entropy, Information and Computing* (Adam Hilger, Bristol, UK, 1990).
19. R. P. Feynman, R. B. Leighton, M. Sands, *The Feynman Lectures on Physics* (Adison-Wesley, Reading, MA, 1966), vol. I, chap. 46.
20. C. Joachim and J. K. Gimzewski, *Proc. IEEE* **86**, 184 1998).
21. A. Aviram and M. A. Ratner, *Chem. Phys. Lett.* **29**, 277 (1974).
22. B. C. Stipe, M. A. Rezaei, W. Ho, *Science* **279**, 1907 (1998).
23. We thank P. Guéret and M. Welland for useful discussions, and A. K. Lay for help in the chemical synthesis. Supported by the European Union ESPRIT project "Nanowires," which is partially funded by the Swiss Federal Office for Education and Science.

Exploiting Chemical Libraries, Structure, and Genomics in the Search for Kinase Inhibitors

Nathanael S. Gray, Lisa Wodicka, Andy-Mark W. H. Thunnissen, Thea C. Norman, Soojin Kwon, F. Hernan Espinoza, David O. Morgan, Georjana Barnes, Sophie LeClerc, Laurent Meijer, Sung-Hou Kim, David J. Lockhart, Peter G. Schultz*

Selective protein kinase inhibitors were developed on the basis of the unexpected binding mode of 2,6,9-trisubstituted purines to the adenosine triphosphate–binding site of the human cyclin-dependent kinase 2 (CDK2). By iterating chemical library synthesis and biological screening, potent inhibitors of the human CDK2–cyclin A kinase complex and of *Saccharomyces cerevisiae* Cdc28p were identified. The structural basis for the binding affinity and selectivity was determined by analysis of a three-dimensional crystal structure of a CDK2-inhibitor complex. The cellular effects of these compounds were characterized in mammalian cells and yeast. In the latter case the effects were characterized on a genome-wide scale by monitoring changes in messenger RNA levels in treated cells with high-density oligonucleotide probe arrays. Purine libraries could provide useful tools for analyzing a variety of signaling and regulatory pathways and may lead to the development of new therapeutics.

Biomedical research has been aided tremendously by three developments: (i) the ability to generate small molecule libraries using combinatorial chemistry methods coupled with high-throughput screening, (ii) the enormous increase in the number of newly identified gene sequences from a host of different organisms, and (iii) the use of structural methods for the detailed characterization of ligand-protein interaction sites that can be exploited for ligand design. Here we applied these methods to the synthesis and characterization of potent, selective inhibitors of protein kinases involved in cell cycle control. The central role that cyclin-dependent ki-

nases (CDKs) play in the timing of cell division and the high incidence of genetic alteration of CDKs or deregulation of CDK inhibitors in a number of cancers make CDKs a promising target for the design of selective inhibitors. Our approach to inhibiting CDKs has been to block the adenosine triphosphate (ATP)–binding site with compounds derived from combinatorial libraries of 2,6,9-trisubstituted purines. This strategy was motivated by the binding mode of the purine olomoucine, which exhibits good selectivity but only moderate inhibition [IC_{50} (50% kinase inhibition) = 7 μM] of a subset of the CDK family of protein kinases (*1*). The orientation of the purine ring of olomoucine within the ATP-binding site of CDK2 is rotated almost 160° relative to that of the adenosine ring of ATP. Thus, it seemed that the introduction of new substituents at the 2, 6, and 9 positions of the purine ring, rather than substituents appended to the ribose, as is normally done, might lead to enhanced binding affinity and selectivity. A combinatorial approach to modifying the purine scaffold could be valuable in the search for potent and selective inhibitors of various cellular processes because of the ubiquitous occurrence of enzymes that use purines, including the estimated 2000 kinases encoded in the human genome.

N. S. Gray, T. C. Norman, S. Kwon, P. G. Schultz, Howard Hughes Medical Institute, University of California, Berkeley, CA 94720, USA. L. Wodicka and D. J. Lockhart, Affymetrix, 3380 Central Expressway, Santa Clara, CA 95051, USA. A.-M. W. H. Thunnissen and S.-H. Kim, Lawrence Berkeley National Laboratory and Department of Chemistry, University of California, Berkeley, CA 94720, USA. F. Hernan Espinoza and D. O. Morgan, Department of Physiology, University of California, San Francisco, CA 94143–0444, USA. G. Barnes, Department of Molecular and Cellular Biology, University of California, Berkeley, CA 94720, USA. S. LeClerc and L. Meijer, CNRS, Station Biologique, 29682 Roscoff, France.

*To whom correspondence should be addressed.

To examine the effects of a range of diverse substituents on the purine ring, we synthesized combinatorial libraries in which the 2, 6, and 9 positions could be varied starting with a 2-fluoro-6-chloropurine framework (Fig. 1A) (2, 3). Substitution chemistry was used to install amines at the 2 and 6 positions,
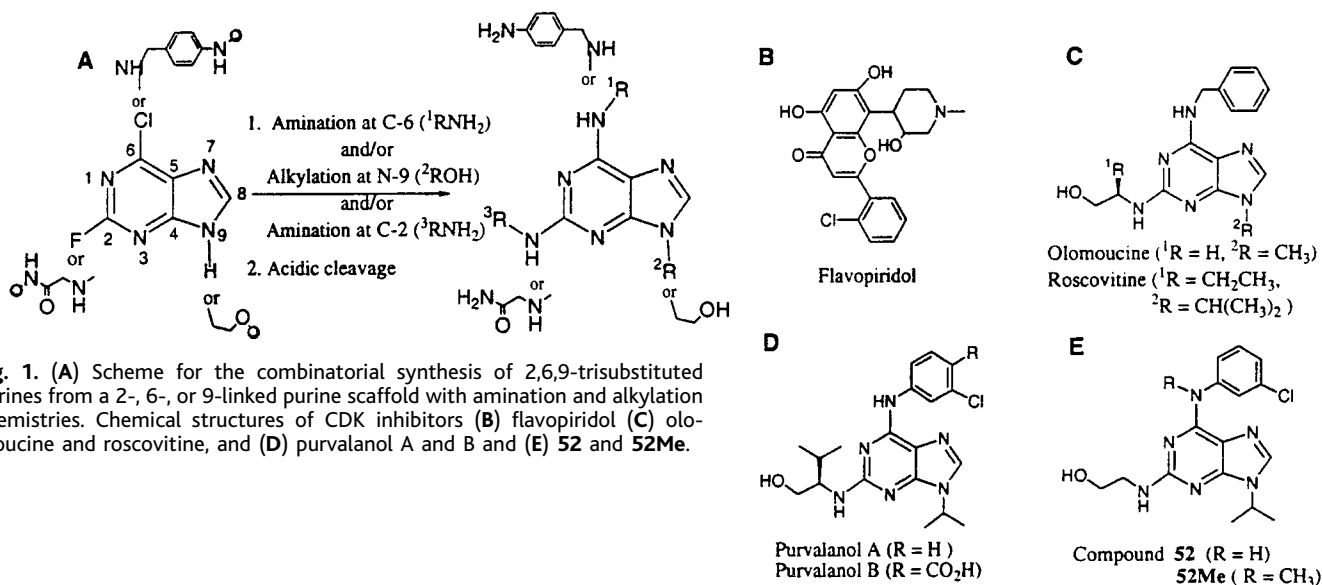
and a Mitsunobu reaction (4, 5) was used to alkylate the N9 position of the purine core. The substitution chemistry allows introduction of primary and secondary amines bearing a wide range of functional groups, whereas the Mitsunobu reaction tolerates primary and secondary alcohols lacking additional acidic hydrogens. Newly appended groups can be modified combinatorially in subsequent steps with a variety of chemistries including acylation, reductive amination, and Suzuki coupling reactions (6). During library synthesis, one position is held invariant to allow attachment to the solid support. Libraries are synthesized in a spatially separated format with either a pin apparatus (7) or polystyrene resin and screened for kinase inhibitors with a 96-well, solution-phase phosphorylation assay.

Several purine libraries in which the 2, 6, and 9 substituents were varied separately were iteratively synthesized and screened. We identified aA number of 3- and 4-substituted benzylamine and aniline substituents that lead to significant improvements in CDK2 binding when introduced at the 6 position of the purine ring. For example, replacement of the benzylamino group of olomoucine at the C6 position with 3-chloroaniline resulted in a 10-fold increase in the IC_{50}. Although a variety of hydroxyalkylamino, dihydroxyalkylamino, and cycloalkylamino substituents at the 2 position resulted in moderate improvements in binding affinity, greater increases were achieved with amino alcohols derived from alanine, valine, and isoleucine. For example the R-isopropyl side chain of valinol resulted in a 6.5-fold increase relative to the hydroxyethyl substituent of olomoucine. In contrast to many protein kinases that can accommodate larger substituents at the N9 of the purine ring, CDK2 binding was strongest for those purines bearing small al-

kyl or hydroxyalkyl substituents. Those substituents that resulted in the most potent CDK2 inhibition were combined in second-generation libraries by solution-phase chemistry. The IC_{50} data for these series of compounds indicate that the inhibitory effects of these substituents are approximately additive.

Currently, our most potent inhibitor, 2-(1R-isopropyl-2-hydroxyethylamino)-6-(3-chloro-4-carboxyanilino)-9-isopropylpurine (purvalanol B, Fig. 1D), has an IC_{50} against the complex of CDK2-cyclin A of 6 nM, which corresponds to a 1000-fold increase over olomoucine and a 30-fold increase over flavopiridol (Fig. 1B), one of the most potent and selective CDK2 inhibitors known and currently in human clinical trials (8). Purvalanol B shows a high degree of selectivity: among the 22 human purified kinases tested (1, 9), only a subset of the CDKs (cdc2-cyclin B, CDK2-cyclin A, CDK2-cyclin E, CDK5-p35) were significantly inhibited (Table 1). Several close analogs of purvalanol B were also potent inhibitors of cdc2 and CDK2, including the more membrane permeable analog purvalanol A and compound **52** [(2-(2-hydroxyethylamino)-6-(3-chloroanilino)-9-isopropylpurine, IC_{50} = 340 nM against cdc2-cyclin B] (Fig. 1E, Table 2). We also assessed the selectivity of purvalanol A, compound **52**, and a N6-methylated version of compound **52** (**52Me**) against four yeast CDKs (10) (Cdc28p, Kin28p, Pho85p, and Srb10p) and the related kinase Cak1p using kinase assays performed in immunoprecipitates (Table 2) (11). Of the yeast kinases tested, only the cell cycle–regulating kinase Cdc28p and the highly homologous Pho85p kinase (50% identity to Cdc28p), which is involved in phosphate metabolism, were inhibited by purvalanol A and **52**. Compound **52Me** did not inhibit any of the CDKs tested.

To explore the structural basis for the selectivity and affinity of these inhibitors we

Table 1. IC_{50} values for purvalanol (purv.) A and B for a variety of purified kinases.

Kinase	Purv. A (IC_{50} nM)	Purv. B (IC_{50} nM)
cdc2-cyclin B	4	6
cdc2-cyclin B (150 μM ATP)	40	50
cdc2–cyclin B (1.5 mM ATP)	500	250
cdk2-cyclin A	70	6
cdk2-cyclin E	35	9
cdk4-cyclin D1	850	>10,000
cdk5-p35	75	6
erk1	9,000	3,333
c-jun NH_2-terminal kinase	>1,000	>10,000
Protein kinase C α	>10,000	>100,000
Protein kinase C β1	>10,000	>100,000
Protein kinase C β2	>10,000	>100,000
Protein kinase C γ	>10,000	>100,000
Protein kinase C δ	>100,000	>100,000
Protein kinase C ϵ	>100,000	>100,000
Protein kinase C η	>100,000	>100,000
Protein kinase C ζ	>100,000	>100,000
cAMP-dependent protein kinase	9,000	3,800
cGMP-dependent protein kinase	>10,000	>100,000
Casein kinase 1	>3,333	>3,333
GSK3-β	>10,000	>10,000
Insulin-receptor tyrosine kinase	5,000	2,200
cCasein kinase 2	>10,000	>10,000
Raf kinase	>1,000	>10,000
v-abl	>10,000	>100,000
cdc28 (S. cerevisiae)	80	1,200

Fig. 1. (A) Scheme for the combinatorial synthesis of 2,6,9-trisubstituted purines from a 2-, 6-, or 9-linked purine scaffold with amination and alkylation chemistries. Chemical structures of CDK inhibitors **(B)** flavopiridol **(C)** olomoucine and roscovitine, and **(D)** purvalanol A and B and **(E) 52** and **52Me**.

determined the crystal structure of the human CDK2-purvalanol B complex to 2.05 Å resolution (12) (Fig. 2). The electron density map shows that binding of purvalanol B to the CDK2 crystals is well ordered except for the 3-chloroanilino group, which appears to be bound in two alternative conformations (Fig. 2). Purvalanol B fits snugly into the ATP-binding site, as is evident by the 86% complementarity between the surface area buried by the inhibitor (364 Å^2) compared with the available binding surface in the active site of the protein (423 Å^2). The overall geometry of purvalanol B bound to CDK2 resembles that of the related adenine-substituted inhibitors in the CDK2-olomoucine and CDK2-roscovitine complexes, with the purine ring and its C2, N6, and N9 substituents occupying similar binding pockets. The purine ring makes mostly hydrophobic and van der Waals contacts with CDK2 residues. A pair of conserved H bonds are present between the N7 imidazole nitrogen and the backbone NH of Leu[83], and between the N6 amino group and the backbone carbonyl of Leu[83]; this latter interaction likely accounts

for the greatly reduced inhibitory activity resulting from methylation of N6 in compound **52Me**. Furthermore, all three 2,6,9-trisubstituted adenines form a H bond between the acidic C8 atom of the purine ring and the carbonyl oxygen of Glu[81], an infrequently observed interaction in the crystal structures of nucleic acids and proteins (13).

The C2 side chain of purvalanol B is bound in the ATP ribose–binding pocket (Fig. 2A, structure 3), with the R-isopropyl group closely packed against backbone atoms of the glycine-rich loop and the hydroxyl group making a H bond with the backbone carbonyl of Gln[131]. The R-isopropyl side chain of purvalanol B leads to a significant repositioning of the C2 substituent relative to the R-ethyl substituent of roscovitine (Fig. 2A, structure 1), resulting in an open pocket in the active site lined by the polar side chains of Lys[33], Asn[132], and Asp[145]. In the CDK2-flavopiridol complex, this region is occupied by the N-methylpiperidinyl ring of the inhibitor (Fig. 2A., structure 2), suggesting that further increases in affinity of purvalanol B may result from appending substituents at the

C2 position that interact with this site. The 3-chloroanilino group at N6 of purvalanol B points toward the outside of the ATP-binding pocket, a region not occupied in the CDK2-ATP complex. Interactions in this region are likely responsible for the increased affinity and selectivity of the inhibitors compared with ATP and are evident in the CDK2 complexes of flavopiridol, olomoucine, and roscovitine as well. In the CDK2-purvalanol B complex, the 3-chloroanilino group of the inhibitor is packed tightly against the side chains of Ile[10] and Phe[82]. Further stabilization of the binding of the 3-chloroanilino group comes from a polar interaction between the Cl and the side chain of Asp[86], which appears to be present in about two-thirds of the molecules in the CDK2-purvalanol B crystals. In the other conformation the phenyl ring of the 3-chloroanilino group is flipped ~160°, suggesting a partially protonated state of Asp[86]. In addition to improved packing interactions, the increased binding affinity of purvalanol B relative to olomoucine may result from steric constraints imposed by the purine and chlorinated aniline ring systems that limit the number of conformations of the inhibitor. Numerous substituents at the 4 position of the aniline ring were tolerated, consistent with the solvent accessibility of this site, which makes this position an obvious candidate for altering both the solubility and membrane permeability. Finally, the N9 isopropyl group of purvalanol B packs in a small hydrophobic pocket formed by the side chains of Val[18], Ala[31], Phe[80], Leu[134], and Ala[144], consistent with the narrow range of substituents that can be tolerated at this position.

To determine the cellular effects of these CDK-directed cell cycle inhibitors, we tested purvalanol A on the NCI panel of 60 human tumor cell lines (leukemia, non–small cell lung cancer, colon cancer, renal cancer, prostate cancer, and breast cancer). Although the average GI$_{50}$ (50% growth inhibition) is 2 μM, two cell lines out of the 60 showed an ~20-fold increase in sensitivity to purvalanol A: the KM12 colon cancer cell line with a GI$_{50}$ of 76 nM and the NCI-H522 non–small cell lung cancer cell line with a GI$_{50}$ of 347 nM. Fluorescence-activated cell sorting (FACS) analysis of human lung fibro-
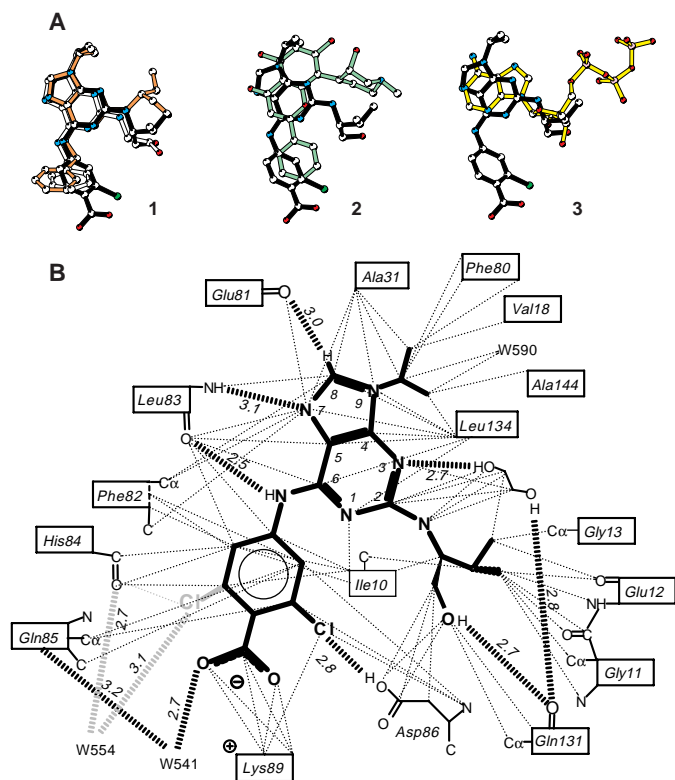
Fig. 2. (A) Purvalanol B bound to CDK2 (black sticks, principal conformation only) is compared with bound (**1**) olomoucine (white sticks) and bound roscovitine (orange sticks), (**2**) bound flavopiridol (green sticks), and (**3**) bound ATP (yellow sticks). The comparisons are based on superposition of the Cα atoms of CDK2. The ligands are shown in ball-and-stick representation with carbon atoms colored white, nitrogen atoms colored blue, oxygen atoms colored red, phosphorous atoms colored violet, and the chlorine atom of purvalanol colored green. (**B**) Schematic drawing of CDK2-purvalanol B interactions. Protein side chain contacts are indicated by lines connecting the respective residue box and interactions to main chain atoms are shown as lines to the specific main chain atoms. Van der Waals contacts are indicated by thin dotted lines, and H bonds by dashed lines. For H bonds the distances between the nonhydrogen atoms are indicated in angstroms. W, water.

Table 2. IC$_{50}$ values for **52** and **52Me** for immunoprecipitated yeast kinases.

Kinases	52 (IC$_{50}$ μM)	52Me (IC$_{50}$ μM)
Cdc28p	7	>500
Pho85p	2	>500
Kin28p	>500	>500
Srb10	>500	>500
Cak1p	>500	>500

blast cells treated with a structural analog of purvalanol A, 2-(bis-(hydroxylethyl) amino)-6-(4-methoxybenzylamino)-9-isopropylpurine, exhibited both G_1-S and G_2-M inhibitory activity at high concentrations and predominant G_1-S inhibition at lower concentrations (*14*). Significant inhibition was also observed in *Saccharomyces cerevisiae*, where compound **52** inhibited growth in a drug-sensitized yeast strain (*15*) with a GI_{50} of 30 µM. In contrast, the closely related compound **52Me** proved to be a significantly weaker inhibitor of yeast growth (GI_{50} = 200 µM) (*16*).

In addition to measuring the inhibitory effects of these purine derivatives in kinase assays and assays of cell growth, their effects on the mRNA levels of nearly all yeast genes were determined with high-density oligonucleotide expression arrays (*17, 18*). These arrays (*19, 20*) make it possible to measure quantitatively and in parallel mRNA levels for a very large number of genes after chemical, environmental, or genetic perturbation. Because purvalanol analogs inhibit both human and *S. 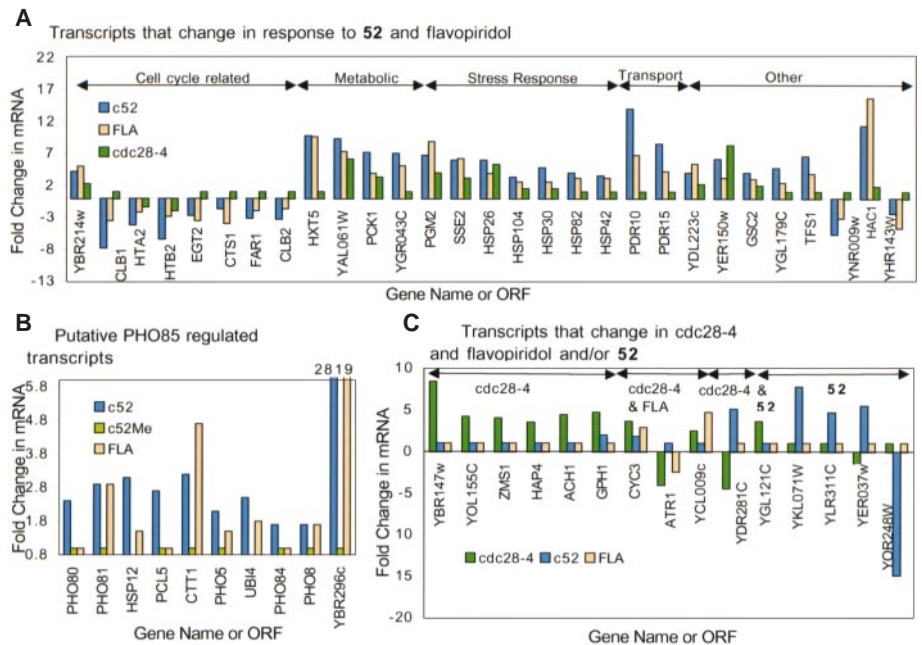cerevisiae* CDKs, transcript profiles were obtained in yeast, where they can be measured on a genome-wide scale. Compounds **52** and flavopiridol were profiled to examine the effects of two structurally different Cdc28p active site inhibitors on gene expression. Compound **52Me** was profiled as a control to determine which transcriptional changes result from treatment with a structurally similar compound with greatly diminished CDK activity. Yeast cultures were grown to late logarithmic phase (*15*), treated with 25 µM concentrations of the inhibitors for 2 hours, after which cellular polyadenylated mRNA was isolated and converted to biotin-labeled complementary RNA (cRNA) (*17, 18*). The labeled cRNA was then hybridized to a set of four arrays containing more than 260,000 25-nucleotide oligomers (*20*).

Out of more than 6200 genes monitored, 194 (3% of transcripts), 2 (0.03% of transcripts), and 132 (2% of transcripts) showed a greater than twofold change in transcript level when treated with **52, 52Me,** or flavopiridol, respectively (*21*). Consistent with the diminished activity of **52Me** both in vivo and in vitro, far fewer transcripts were affected by compound **52Me** than by the CDK inhibitors. Of the 63 transcripts that changed in response to both CDK inhibitors **52** and flavopiridol, only nine were down-regulated, five of which (*CLB1, CLB2, HTA2, HTB2, EGT2*) were associated with cell cycle progression (Fig. 3A). The transcript encoded by *CLB1* (G2 cyclin, implicated in the transition into mitosis) showed a significant decrease, consistent with inhibition of the Cdc28p-Clb1/2p kinase, which is involved in a positive feedback loop driving *CLB1/2* transcription (*22*). Similarly, CDK activity has been implicated in transcriptional regulation of histone genes including *HTA2* and *HTB2* (*23*), and *EGT2*, a gene involved in the timing of cell separation after cytokinesis.

Another set of genes that are clearly affected by both **52** and flavopiridol (but not by **52Me**) are ones involved in phosphate metabolism, consistent with the observed in vitro inhibition of Pho85p (Fig. 3B). Intracellular phosphate levels in yeast are monitored by a system that relies on the Pho85p kinase complex to modulate the activity of a transcription factor or factors that regulate a va-

Fig. 3. Representative transcripts observed to change more than twofold for triplicate hybridizations for each of two independent experiments (except for cdc28-4, which represents triplicate hybridizations of RNA from a single experiment). (**A**) Names of the genes whose mRNA levels change in common to **52** and flavopiridol (none of these transcripts changed significantly in the **52Me** profile): YBR214w (similar to *Schizosaccharomyces pombe* protein moc1 involved in meiosis and mitosis); YGR108W (*CLB1*, G_2-M phase cyclin); YBL003c (*HTA2*, histone); YBL002w (*HTB2*, histone); YNL327W (*EGT2*, involved in timing of cell separation); YLR286C* (*CTS1*, endochitinase); YJL157C* (*FAR1*, inhibitor of Cdc28p/Cln1,2p complexes); YPR119W* (*CLB2*, G_2-M phase cyclin); YHR096C (*HXT5*, homologous to hexose transporters); YAL061W (unknown, similar to alcohol or sorbitol dehydrogenase); YKR097W (*PCK1*, phosphoenol pyruvate carboxykinase); YGR043C (similar to Tal1p, a transaldolase); YMR105C (*PGM2*, phosphoglucomutase); YBR169c (*SSE2*, heat shock protein of HSP70 family); YBR072W (*HSP26*, heat shock protein induced by osmostress); YLL026W (*HSP104*); YCR021c (*HSP30*); YPL240C (*HSP82,* chaperonin homologous to *Escherichia coli* HtpG);

YDR171W (*HSP42*, involved in restoration of cytoskeleton during mild stress); YOR328W (*PDR10*, member of the ATP binding cassette superfamily); YDR406w (*PDR15*); YDL223c (unknown); YER150w (similar to Sed1p an abundant cell surface glycoprotein); YGR032W (*GSC2*, component of β-1,3-glucan synthase); YGL179C* (serine-threonine kinase similar to Elm1p and Kin82p); YLR178C (*TFS1*, Cdc25-dependent nutrient and ammonia response cell cycle regulator); YNR009W (unknown); YFL031W (*HAC1*, basic leucine zipper protein, activates unfolded-protein response pathway); and YHR143W (unknown). (**B**) Transcript changes that may result from Pho85p kinase inhibition observed in either the **52** or flavopiridol profiles: YOL001W (*PHO80*, a cyclin that associates with Pho85p); YGR233C (*PHO81*, inhibitory protein that associates with Pho80p or Pho85p); YFL014W (*HSP12*, heat shock protein); YHR071W (*PCL5*, cyclinlike and associates with Pho85p); YGR088W (*CTT1*, cytosolic catalase T); YBR093C (*PHO5*, secreted acid phosphatase); YLL039c (*UBI4*, ubiquitin); YCL009c (*PHO84*, phosphate transporter); YML116W (*PHO8*, vacuolar alkaline phosphatase); YBR296c (homologous to a phosphate-repressible permease). (**C**) Transcripts that change for cdc28-4, cdc28-4 and **52**, cdc28-4 and flavopiridol, and **52**: YBR147W (unknown, has 7 potential transmembrane domains); YOL155C (unknown, similar to glucan 1,4-α-glucosidase); YJR127C (*ZMS1*, similar to Arp1p, an *N*-acetyltransferase); YKL109W (*HAP4*, transcriptional activator protein involved in activation of CCAAT box–containing genes); YBL015w (*ACH1*, acetyl-coenzyme A hydrolase); YPR160W (*GPH1*, glycogen phosphorylase); YAL039C (*CYC3*, cytochrome c heme lyase); YML116W (*ATR1*, member of major facilitator superfamily); YCL009c (*ILV6*, acetolactate synthase regulatory subunit); YDR281C (unknown); YGL121C (unknown); YKL071w (unknown, similar to bacterial protein csgA); YLR311C (unknown); YER037w (unknown); YOR248W (unknown). *Names marked by an asterisk indicate open reading frames for which at least one hybridization of the set indicated a slightly less than twofold change in abundance.

riety of genes, including a secreted acid phosphatase (Pho5p) (24), genes involved in the stress response (the heat shock protein HSP12 and ubiquitin UBI4), and genes involved in glycogen metabolism. Proteins whose transcript levels were observed to increase for 52 or flavopiridol that are consistent with inhibition of the Pho85p kinase include Pho80p (whose transcription is known to be repressed by active Pho85), Pho81p (an endogenous Pho85-Pho80 inhibitor), Pho84p (a phosphate permease), Pho5p, CTT1p, HSP12p, and UBI4 (25). Notably absent from this list is glycogen synthase (GSY2) (26), despite the large number of other glycogen metabolism mRNAs that change. Dissecting the transcriptional consequences of Pho85 inhibition (27) is additionally complicated because Pho85p associates with a large number of other cyclins (for example, Pcl1p-Pcl8p) (28) to yield complexes of unknown function that may also be subject to inhibition.

Compound 52 and flavopiridol also affect the transcript levels of many genes involved in cellular metabolism. For example, genes involved in glycolysis (PFK26 and YAL061W, an alcohol dehydrogenase), the citric acid cycle (ALD4), glycogen metabolism (PGM2 and YPR184W, a putative debranching enzyme), gluconeogenesis (PCK1), and a probable sugar transporter (HXT5), were induced. Other changes in transcript levels that were in common to both compounds and are likely to be associated with drug exposure include up-regulation of a number of genes encoding members of the ATP-binding cassette superfamily and other transport proteins (PDR10, PDR15), cell wall glycoproteins (YER150w), and cell wall proteins implicated in increased drug resistance (GSC2) (29); genes involved in vacuole endocytosis and regulation (YPT53, PMC1); and several heat shock genes (HSP26, HSP30, HSP82, HSP104, SSE2). Additional genes with changes in common to both compounds include a GTP- and ATP-binding protein (YDL223c) that putatively binds microtubules, l-myo-inositol-1-phosphate synthase (INO1), and 40 genes of unknown function. Very few of the 52 and flavopiridol-inducible genes were significantly induced by 52Me, suggesting that many of the drug-sensing mechanisms may respond to signals associated with the function rather than the structure of the drug.

Although Cdc28p is the intended target of both 52 and flavopiridol, more than half of the mRNA changes that result from exposure to the two compounds are distinct. For example, of the ~50 genes whose transcript levels were decreased at least threefold in response to 52, 14 were ribosomal proteins (including RPL4A, RPL26B, RPS24A). In contrast, no ribosomal protein transcript levels decreased more than threefold after treatment with fla-

vopiridol. These results suggest that the two compounds may inhibit Cdc28p function (10) or affect pathways involving Cdc28p kinase activity to different degrees. Alternatively, the differential effects of the two compounds may result from different intracellular concentrations or from their effects on other cellular targets not specifically examined in vitro. Given the relatively large number of transcripts that are differentially affected by these two CDK inhibitors, we examined the transcriptional consequences of a genetic mutation in the Cdc28p kinase. Because CDC28 is an essential gene, the transcript profile of two cdc28 temperature-sensitive alleles [cdc28-4 and cdc28-13 (30)] and their isogenic wild-type strains were measured under permissive growth conditions (25°C) in which the degree of growth inhibition approximates that observed at the concentrations used in the inhibitor profile experiments (31). The mutation leading to a reduction in Cdc28p kinase activity in the cdc28-4 mutant under permissive growth conditions (32) might be expected to simulate the effects of chemical inhibition.

Approximately 100 mRNAs in the cdc28-4 strain exhibited more than twofold inductions over the wild type (Fig. 3C). Only two of the cell cycle–associated genes (histones HTA1 and HTA2) that changed in response to flavopiridol or 52 were affected in this mutant (33). Instead, as with flavopiridol and 52, a number of metabolic genes involved in glycogen synthesis, the citric acid cycle, gluconeogenesis, and the glyoxylate cycle were induced (Fig. 3C). Consistent with these changes is the induction of the HAP4 transcription factor, which has been implicated in the regulation of many respiration genes (34). Another class of transcripts induced in cdc28-4 were for genes involved in stress signaling (35), as well as heat shock elements, stress response elements, and members of the major facilitator superfamily. Other transcripts that were also affected by CDC28 mutation and in the small-molecule experiments include virtually all of the transcription factors and many of the metabolic, biosynthetic, and stress response genes as well as a set of unknown genes, some of which may be linked to cell cycle regulation. However, there were also a number of genes in these functional categories that showed significant changes only for the cdc28-4 mutant, including a protein with transmembrane domains (YOL155C), metabolic genes (ACH1), and a variety of proteins of unknown function. The transcriptional responses to this single point mutation in CDC28 can be interpreted as cellular responses that tend to mitigate the effects of this alteration. Complete inactivation of Cdc28p kinase activity, rather than the partial inhibition at 25°C, may result in more cell cycle–related transcript changes. However, a host of additional

changes associated with cell cycle arrest and secondary consequences of heat shock (required to induce arrest) are likely to appear as well, and these changes may complicate interpretation of the profile results.

Our current experimental design does not allow us to definitively identify the primary target or targets of inhibition by flavopiridol or 52. However, most of the genes that were commonly down-regulated by the two compounds are known to be involved in cell cycle progression and are affected in a way that is consistent with inhibition of Cdc28p activity. The transcript profiles also show distinct and reproducible differences in the effects of the two compounds despite their similar in vitro activity. Profiles of this sort may prove useful in evaluating the selectivity of drug candidates and in identifying proteins whose inhibition might specifically potentiate the effects of a primary drug. The lack of correspondence in the changes of mRNA transcript levels resulting from chemical and genetic inactivation underscores the intrinsic differences in these methods for modulating biological function.

Given the large number of purine-dependent cellular processes, purine libraries may serve as a rich source of inhibitors for many different protein targets. Indeed, purine analogs have been identified that selectively inhibit JNK kinase and glycogen synthase kinase (36, 37). By screening these libraries for their effects in whole-cell assays, it should be possible to search for compounds with a wide variety of activities (38). Both gene expression profiles and differential gene expression libraries should facilitate identification and characterization of targets (39). These and other approaches to generating selective inhibitors of different cellular processes should complement genetic methods in the study of cellular function.

References and Notes

1. J. Vesely et al., Eur. J. Biochem. 224, 771 (1994); L. Meijer et al., ibid. 243, 527 (1997).
2. N. S. Gray, S. Kwon, P. G. Schultz, Tetrahedron Lett. 38, 1161 (1997).
3. T. C. Norman, N. S. Gray, J. T. Koh, J. Am. Chem. Soc. 118, 7430 (1996).
4. O. Mitsonobu, Synthesis 1, 1 (1981).
5. A. Toyota, N. Katagiri, C. Kaneko, Heterocycles 36, 1625 (1993).
6. B. J. Backes and J. A. Ellman, J. Am. Chem. Soc. 116, 11171 (1994).
7. H. M. Geysen, S. J. Rodda, T. J. Mason, G. Tribbick, P. G. J. Schoofs, Immunol. Methods 102, 259 (1987).
8. L. Meijer, Trends in Cell Biol. 6, 393 (1996).
9. Starfish is the major source for cdc2-cyclin B kinase. The recombinant human cdc2-cyclin B is likely to contain inactive monomers and dimers that would interfere with CDK inhibition assays [see (11)].
10. D. O. Morgan, Annu. Rev. Cell Dev. Biol. 13, 261 (1997).
11. Supplemental material is available at www.sciencemag.org/feature/data/976815.shl.
12. Crystallography statistics for the CDK-purvalanol B complex. Data: space group, P212121, cell constants a = 53.55 Å, b = 71.35 Å, c = 72.00 Å, resolution 32 to 2.05 Å. Number of unique reflections = 17655,

completeness = 98.7% (91.6 from 2.11 to 2.05 Å), $R_{merge} = \Sigma_h \Sigma_i |I_{hi} - \langle I_h \rangle| / \Sigma_h \Sigma_i |I_{hi}| = 5.5\%$, where h are unique reflections indices and i indicate symmetry equivalent indices. Refinement calculations: $R_{factor} = (\Sigma |F_o - F_c|)/\Sigma F_o = 18.8\%$, where F_o and F_c are the observed and calculated structure factors, respectively; $R_{free} = 26.4\%$ (same calculation as for R_{factor}, but with 5% of the data); average atomic B values for protein: 31.4 Å^2, inhibitor = 32.2 Å^2, waters = 37.7 Å^2. Observed deviations: root means square (rms) bond lengths = 0.008 Å; rms bond angles = 1.31°. The final model includes 279 residues of CDK2 (residues 36 to 43 and 153 to 163 are not included because of weak or missing electron density), purvalanol B, 91 water molecules, and one molecule of ethyleneglycol. Efforts to crystallize the CDK2-purvalanol A complex resulted crystals of poor quality.
13. M. C. Wahl and M. Sundaralingam, *Trends Biochem. Sci.* **22**, 97 (1997).
14. E. E. Brooks et al., *J. Biol. Chem.* **272**, 29207 (1997).
15. Because of weak inhibition of yeast growth by flavopiridol we used a strain with three drug-sensitizing deletions (Δ*erg6*, Δ*pdr5*, Δ*snq2*). This strain showed GI$_{50}$ for **52** and flavopiridol at concentrations of 30 and 7 μM, respectively. Three cultures [110 ml, in yeast extract, peptone, and dextrose (YPD)] were inoculated with single colonies of YRP1 (*MATα*, Δ*erg6::LEU2*, Δ*pdr5::TRP1*, Δ*snq2::HIS6*) and grown at 30°C with constant agitation in a water bath incubator. When the cell density reached an optical density (OD) of 0.9 (at a wavelength of 600 nm), 27.5 μl of a 100 mM dimethyl sulfoxide (DMSO) stock solution of **52** or flavopiridol or DMSO alone was added. After 2 hours the cells were harvested by centrifugation and flash frozen with liquid nitrogen. For the temperature-sensitive *cdc28* mutants, three cultures (75 ml, YPD) of AFS199 (*cdc28-13*), AA104 (*cdc28-4*), and their isogenic background strain AFS34 (*MATa, ade2-1, his3-11, leu2-3, trp1-1, ura3*) were grown from single colonies to an OD of 0.9 (600 nm) and harvested as described. Frozen cells were stored at −80°C.
16. The diminished growth inhibitory activity of compound **52Me** is unlikely to result from poorer bioavailability because a similar N6 methylation is observed to increase the in vivo potency of a related series of purine-based inhibitors. The residual growth inhibitory activity of **52Me** likely reflects activity against other cellular targets. Compounds **52**, **52Me**, and flavopiridol failed to cause a uniform arrest morphology in yeast. FACS analysis also did not reveal synchronization of yeast cells after treatment with **52** or **52Me**, which may be due to inhibition of a variety CDKs responsible for different cell cycle transitions (as is observed in FACS experiments on mammalian cells) or activity against other targets not specifically examined in vitro.
17. D. J. Lockhart et al., *Nature Biotechnol.* **14**, 1675 (1996).
18. L. Wodicka, H. Dong, M. Mittmann, M.-H. Ho, D. J. Lockhart, ibid. **15**, 1359 (1997).
19. J. L. DeRisi, V. R. Iyer, P. O. Brown, *Science* **278**, 680 (1997).
20. S. P. A. Fodor et al., ibid. **251**, 767 (1991).
21. Transcripts that showed a significant and reproducible change in concentration (greater than twofold) in cells treated with the compounds between triplicate hybridizations for each of at least two independent experiments were examined further.
22. F. R. Cross, *Curr. Opion. Cell Biol.* **7**, 790 (1995).
23. A. J. Van Wijnen et al., *Proc. Natl. Acad. Sci. U.S.A.* **91**, 12882 (1994).
24. E. M. Lenburg and E. K. O'Shea, *Trends Biol. Sci.* **V21** 383 (1996).
25. L. W. Bergman and B. K. Timblin, *Mol. Microbiol.* **26**, 981 (1997).
26. L. W. Bergman, K. Tatchell, B. K. Timblin, *Genetics* **143**, 57 (1996).
27. Because the *PHO85* gene is nonessential it should be possible to determine if these inductions are a direct consequence of Pho85p kinase inhibition by determining if the same inductions are seen after treating with inhibitor in a strain lacking the kinase.
28. B. Andrews et al., *Mol. Cell Biol.* **17**, 1212 (1997).
29. P. Mazur et al., ibid. **15**, 5671 (1995).
30. Transcript profiles were also measured for the *cdc28* temperature-sensitive allele *cdc28-13*. The *cdc28-13* strain contains an arginine to asparagine mutation at residue 283 near the COOH-terminus, which does not significantly affect kinase activity at the permissive temperature but does cause cell cycle arrest when switched to the nonpermissive temperature (*32*). The *cdc28-13* strain showed very few changes in mRNA transcripts when compared with wild type at the permissive temperature. The levels of only 11 mRNAs changed by more than twofold, consistent with the observation that this mutant has essentially wild-type kinase activity at 25°C. In addition, the nearly identical gene expression patterns obtained for the *cdc28-13* and isogenic wild-type *CDC28* strain demonstrate the reproducibility of these experiments.
31. The *cdc28-4* allele that exhibits a START (G$_1$-S) defect or an allele such as *cdc28-1N*, which has a G$_2$-M defect could also serve as a mimic of CDK inhibition by **52** or flavopiridol.
32. S. I. Reed, J. A. Hadwiger, A. T. Lorincz, *Proc. Natl. Acad. Sci. U.S.A.* **82**, 4055 (1985).
33. C. Koch and K. Nasmyth, *Curr. Opion. Cell Biol.* **6**, 451 (1994).
34. M. Russell, J. Bradshaw-Rouse, D. Markwardt, W. Heideman, *Mol. Biol. Cell* **4**, 757 (1993).
35. H. Ruis and C. Schuller, *BioEssays* **17**, 959 (1995).
36. J. R. Woodgett et al., *Trends Biochem. Sci.* **16**, 177 (1991).
37. U.S. Patent Application 1368.002
38. For example, using a screen of our purine libraries, to be described elsewhere, we have identified a compound that causes extensive depolymerization of microtubules and condensation of DNA.
39. J. Rine, W. Hansen, E. Hardeman, R. W. Davis, *Proc. Natl. Acad. Sci. U.S.A.* **80**, 6750 (1983); M. Schena, D. Shalon, R.W. Davis, P. O. Brown, *Science* **270**, 467 (1995).
40. We thank A. Murray for providing the CDC28 temperature-sensitive strains and for helpful discussions, C. Mimotopes for providing derivatized pins, D. Drubin and members of his lab, the National Cancer Institute for performing cellular screens, and M.-H. Ho for help with expression data analysis. Supported by the Director, Office of Health Effects Research of the U.S. Department of Energy (to S.-H. K. and P.G.S.), the Association pour la Recherche sur le Cancer (ARC9157 to L.M.), the Counsil Regional de Bretagne (to L.M.), and the CaP Cure Foundation. N.S.G. is supported by a NSF predoctoral fellowship and A.-M.T. by a long-term fellowship from the Human Frontier Science Program. The coordinates have been deposited with Protein Data Bank with ID code 1CKP.

22 April 1998; accepted 4 June 1998

Synthesis of Macroporous Minerals with Highly Ordered Three-Dimensional Arrays of Spheroidal Voids

Brian T. Holland, Christopher F. Blanford, Andreas Stein*

Titania, zirconia, and alumina samples with periodic three-dimensional arrays of macropores were synthesized from the corresponding metal alkoxides, using latex spheres as templates. In a fast, single-step reaction, the monomeric alkoxide precursors permeate the array of bulk polystyrene spheres and condense in air at room temperature. Close packed, open-pore structures with 320- to 360-nanometer voids are obtained after calcination of the organic component at 575°C. The examples presented demonstrate the compositional diversity possible with this technique. The resulting highly structured ceramics could have applications in areas ranging from quantum electronics to photocatalysis to battery materials.

The use of organic templates to control the structure of inorganic solids has proven very successful for designing porous materials with pore sizes ranging from angstroms to micrometers. In the case of microporous silicates and aluminosilicates, the organic additives are molecular and lead to zeolitic structures. Larger mesopores are obtained by using surfactant arrays or emulsion droplets as templates (*1–4*). Recent reports illustrate that techniques using latex spheres or block-copolymers can be used to create silica structures with pore sizes ranging from 5 nm to 1 μm (*5–8*). Porous solids have made a great impact in applications including catalysis, sorption, and separations (*9*). Advanced optoelectronics applications that would benefit from a facile method of producing large quantities of porous materials in various compositions with high degrees of three-dimensional (3D) order have been proposed (*10*). For example, quantum electronics and optical communications require single-mode microcavities constructed from dielectric materials with adjustable composition and multidimensional periodicity (*11*). So far, the fabrication of such structures with periodicity in three dimensions and feature sizes below 1 μm has remained an experimental challenge (*12*). Catalysis and large-molecule separation processes would also benefit from more uniform porous supports that provide optimal flow and improved efficiencies (*13, 14*).

Department of Chemistry, University of Minnesota, Minneapolis, MN 55455, USA.

*To whom correspondence should be addressed. E-mail: stein@chem.umn.edu